ELSEVIER

PII: S0032-3861(97)10230-0

Polymer Vol. 39 No. 20, pp. 4827–4834, 1998

0032-3861/98/$19.00+0.00

Elongational flow-induced crystallization in supercooled poly(ethylene terephthalate) with different crystallization habit†

Hiroshi Kubo, Masami Okamoto and Tadao Kotaka*

Advanced Polymeric Materials Engineering, Graduate School of Engineering, Toyota Technological Institute, Hisakata 2-12-1, Tempaku, Nagoya 468, Japan
(Received 11 August 1997; revised 20 October 1997; accepted 23 October 1997)

Elongational flow-induced crystallization behaviour was investigated on supercooled liquids of two poly(ethylene terephthalate)s (PET) with different crystallization habit *via* elongational flow opto-rheometry (EFOR), temperature-modulated differential scanning calorimetry (TMd.s.c.) and Rayleigh scattering in the temperature range of 100–130°C usually employed for blow moulding operations. The samples were an antimony catalysed PET (Sb-PET) with rapid crystallization rate but less-ordered spherulites, and a germanium catalysed PET (Ge-PET) with temperature sensitive (slow) crystallization rate but better organized spherulites. In the elongation of Sb-PET at 110°C, transformation of the spherulites into rod-like morphology occurred even in the early stage, which was followed by a strong *strain hardening* tendency, accompanying the increasing of birefringence. On the other hand, for Ge-PET at 110°C, molecular orientation along the flow direction preceded and then flow-induced crystallization with crystalline lamellae growing transverse to the oriented chains took place rather suddenly at a Hencky strain ε of ≈ 2. However, in Ge-PET elongated at 130°C especially with low strain rate $\dot{\varepsilon}_0$, spherulite growth dominated the rheology. In these PETs, the features of the flow-induced structure development were governed by the dimensionless strain rate that was the ratio of $\dot{\varepsilon}_0$ to the spherulite growth rate under quiescent state. Depending on the dimensionless rate being above or below a certain critical value, the oriented crystallite formation or the spherulite growth dominated the behaviour, respectively.

(Keywords: PET; crystallization rate; elongation)

INTRODUCTION

In our previous papers[1,2], we described elongational flow-induced crystallization of a poly(ethylene terephthalate) (PET) (of a blow moulding grade) revealed *via* elongational flow opto-rheometry (EFOR)[3,4], temperature-modulated differential scanning calorimetry (TMd.s.c.)[1] and Rayleigh scattering. The tests were conducted on its supercooled liquid state in the temperature range of 100–130°C that was comparable to the blow moulding and/or film blowing conditions[5–7]. In the specimen elongated at 100–110°C where spherulite growth was negligible, deviation of the elongational viscosity from the linear relation or so-called *strain-induced hardening* became prevailing after a certain time t_c corresponding to the Hencky strain of $\varepsilon_{\eta E}(=\dot{\varepsilon}_0 t_c) \approx 1$ independent of the Hencky strain rate $\dot{\varepsilon}_0$. The crystallization did not take place until the strain reached a critical value of ε $(=\dot{\varepsilon}_0 t) \approx 2$, beyond which flow-induced oriented crystalline formation took place rather suddenly regardless of $\dot{\varepsilon}_0$. Under such a condition the *Hv* (cross-polarized) scattering yielded two-point patterns parallel to the elongational direction with strong streaks in the perpendicular direction. These results implied that, regardless of $\dot{\varepsilon}_0$, molecular orientation proceeded along the flow direction and beyond ε $(=\dot{\varepsilon}_0 t) \approx 2$, crystalline domains began to grow transverse to the oriented chains[2].

In contrast, at 130°C where spherulite growth was rapid, the critical strain $\varepsilon_{\eta E}$ at the onset of strain-induced hardening varied from ~0.5 to 1.0 as $\dot{\varepsilon}_0$ was increased. In the *Hv* patterns of the sample elongated at 130°C, a four-leaf clover pattern typical to spherulites was observed at the start of elongation $\varepsilon \approx 0$. Even in the intermediate to late stages, especially when elongated with low $\dot{\varepsilon}_0$, spherulite growth surpassed destruction of the spherulites or formation of flow-induced *oriented* crystallite. In such cases a smeared four-leaf clover pattern was observed, implying that the spherulites were deformed[2]. Under these conditions the spherulite growth dominated over oriented-crystallite formation unless $\dot{\varepsilon}_0$ was extremely high. Thus in the elongational flow of supercooled semicrystalline polymer liquids, the difference in the crystallization behaviour, in particular, the spherulite formation behaviour should play a crucial role.

In practical applications of film- and/or bottle-browing, PET resins catalysed with germanium (Ge) or antimony (Sb) were often used, but they were known to exhibit entirely different crystallization behaviour[8]. The PET resin used in the previous study[1] was in fact a Ge-catalysed sample of blow moulding grade. Then we expect that the elongational flow behaviour of an Sb-catalysed PET resin should be different from the behaviour of Ge-catalysed PET. In this paper, we examine the flow-induced crystallization behaviour of PET polymerized with an antimony/magnesium catalyst system and compare the results with those of slowly crystallizing Ge-catalysed PET in supercooled state. Such a comparison will be worthwhile not only for assessing the performance of different PETs in polymer

* To whom correspondence should be addressed
† Elongational Flow Opto-Rheometry for Polymeric Liquids, Part 5

Table 1 Characteristics of the PET resins used in this study

Code	Sb-PET	Ge-PET
Catalyst used	Sb/Mg 160/50 ppm	Ge 50 ppm
$[\eta]$ (dl g^{-1})[a]	0.75	0.77
M_w (kg mol^{-1})	52.1	54.5
M_w/M_n	2.2	2.2
T_g (°C)	~78	~76
T_m (°C)	254	253

[a]Determined in *p*-chlorophenol/1,1,2,2-tetrachloroethane (3/1 v/v) at 30°C

processing operations but also for studying the transformation of crystal texture such as spherulites formed in the early stage of elongation into a new texture of the oriented crystalline form, depending on the flow conditions.

EXPERIMENTAL

Materials and methods

A commercial poly(ethylene terephthalate) (Sb-PET) sample of film-moulding grade, polymerized with an antimony/magnesium catalyst system, was supplied by Toyobo Co. To compare the effect of the crystallization rate on elongational flow behaviour we also tested slowly crystallizing PET (Ge-PET) polymerized with a gerumanium catalyst system. The characteristics of both Sb-PET and Ge-PET resins are listed in *Table 1*. The intrinsic viscosity (η) was determined in a mixture of *p*-chlorophenol/1,1,2,2-tetrachloroethane (3/1 v/v) at 30°C. The glass transition and melting temperatures were determined on a TMd.s.c. at a heating rate of 10°C min^{-1}. The molecular weight M_w and its index of distribution, M_w/M_n, were determned on gel permeation chromatography (g.p.c.) using a mixture of chlorobenzene/*m*-cresol (1/3 v/v) as eluent at 40°C and narrow-distribution polystyrenes as elution standards[9]. The details of EFOR and TMd.s.c. including the method of sample preparation were essentially the same as those described elsewhere for Ge-PET[1–3]. Below we briefly describe the method of sample preparation, because the preheating condition is crucial in testing a specimen on EFOR especially for the sample such as Sb-PET having a rapid spherulite growth rate. First, pellets of both Ge- and Sb-PET were dried under a reduced pressure of 10^{-4} torr at 140°C for 16 h to remove moisture. The pellets were then sandwiched between polyimide films (Kapton®HN, Toray-DuPont) and compression-moulded with a laboratory hot press kept at 290°C ($> T_m$ of PET) for 90 s. The moulded sheet was quenched to room temperature by sandwiching it with glass plates to obtain an amorphous sheet, which was then cut into thin strips of 60 mm × 7 mm × 0.4 mm in size for EFOR measurements. In each EFOR run, an amorphous strip was placed in the sample supporting system set at a desired test temperature between 100 and 130°C, and before starting the measurement annealed *in situ* for 90 s, that is long enough to equilibrate the temperature, but hopefully short enough to suppress the spherulite growth as much as possible. Nevertheless, in readily crystallizable cases such as Sb-PET at 110°C and Ge-PET at 130°C the degree of crystallinity in the unstretched specimen reached as much as 2–5%, as revealed by TMd.s.c. tests (*cf. Figures 6* and *7*).

Crystallization rate under quiescent state

We observed isothermal crystallization behaviour of the PET samples under quiescent state *via* Rayleigh scattering photometry[2]. The light scattering (LS) photometer we used was equipped with a 38 channel photodiode array (PDA: Hamamastu Photonics Co.) and a He–Ne laser of 632.8 nm wavelength. Plane polarized light from the laser source was applied vertically to a sample specimen and the scattering profile was observed at azimuthal angle of 45° under *Hv* (cross-polarized) optical alignment. The LS photometer facilitated time-resolved measurement of LS profiles (the angular dependence of scattered light intensity) within the scattering vector range of 0.37–7.00 μm^{-1} with a time slice of 1/30 s[2].

For LS measurement, dried PET pellets were sandwiched between two pieces of cover glass, placed on a laboratory hot press and compression moulded at 290°C for 90 s to obtain a thin film of thickness ~30 μm. Then the molten film was rapidly quenched to a desired supercooled state at 110–130°C by putting it on a thermostatted hot-stage (Linkam LK600PM, Linkam Scientific Instruments, Ltd) set on the LS photometer. Immediately after the temperature drop, time-resolved LS measurement was carried out as described in the previous articles[2,10,11]. We observed changes of LS profiles with time after the temperature drop at an interval of 1–10 s, depending on the crystallization rate of the specimens.

To analyse the scattering data, we employed integrated scattering intensity, i.e. the invariant Q defined by:

$$Q = \int_0^\infty I(q) q^2 dq \tag{1a}$$

$$q = (4\pi/\lambda)\sin(\theta/2) \tag{1b}$$

where q is the scattering vector corresponding to the scattering angle θ as defined in equation (1), and λ the wavelength of light in the specimen, and $I(q)$ the intensity of the scattered light at q[12].

In the course of spherulite growth or isothermal crystallization under a quiescent state, scattering intensity increases with time, reflecting the increase in optical anisotropy caused by the crystallization. Then the invariant Q for the *Hv* mode is essentially Q_δ, corresponding to the mean-sequare optical anisotropy $\langle\delta^2\rangle$ defined as:

$$Q_\delta \propto \langle\delta^2\rangle \propto \phi_s(\alpha_r - \alpha_t)^2 \tag{2}$$

where ϕ_s is the volume fraction of the spherulites and α_r and α_t are the radial and tangental polarizabilities of the spherulites, respectively[12]. Then we constructed a plot of reduced invariant Q_δ/Q_δ^∞ *versus* time t with Q_δ^∞ being Q_δ at an infinitely long time where crystallization had been completed (it was in fact ~3 h for the present polyester samples). Then taking the *crystallization half-time* $\tau_{1/2}$ at which Q_δ/Q_δ^∞ reaches 1/2, we define $1/\tau_{1/2}$ as a measure of the overall crystallization rate constant. Then we constructed Arrhenius plots of $1/\tau_{1/2}$ *versus* reciprocal of the absolute temparature, $1/T$, for the spherulite growth behaviour.

We also applied the LS photometry to specimens subjected to EFOR to a given extent of elongation to see the elongational flow induced crystallization behaviour. The method of recovering the specimens for such LS photometry was also described elsewhere[2].

RESULTS

Spherulite formation under quiescent state

In order to analyse elongational flow-induced structure development in PET, first we need to know the isothermal crystallization behaviour under quiescent state. Sb-PET is

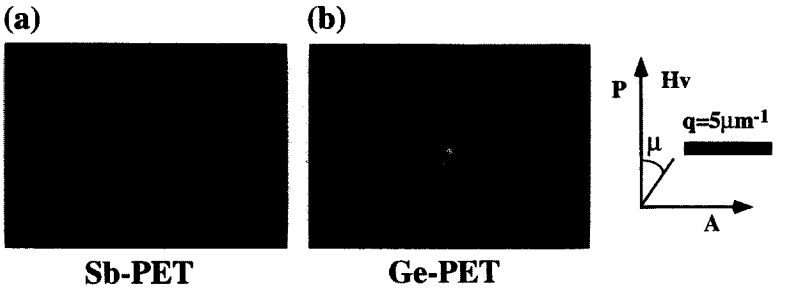

Figure 1 *Hv* light scattering patterns of (a) Sb- and (b) Ge-PET obtained after a long time of isothermal crystallization at 110°C

known to have a rapid overall-crystallization rate because of the rapid nucleation at an extremely large number of sites. However, morphology of the spherulites in Sb-PET is usually less ordered, so that we can hardly follow the growth rate under a polarizing microscope as we have done on Ge-PET[1]. In such a case, time-resolved LS photometry provides a powerful tool for estimating the crystallization rate and its kinetics in supercooled crystalline polymer liquids[10,11].

Figure 1 shows typical examples of LS *Hv*-patterns for (a) Sb-PET compared with (b) Ge-PET, both taken at 110°C after a sufficiently long time of annealing (~1 h for the former and ~3 h for the latter) by which time spherulite growth has been completed and the spherulites may cover all the field of a microscope. In *Figure 1a* for Sb-PET, a large smeared four-leaf-clover pattern is observed, suggesting the formation of a large number of less-ordered spherulites as compared with that in crystallized Ge-PET shown in *Figure 1b*. In the former the locations and intensities of scattering maxima along the azimuthal angle μ are not so obvious even in such a late stage of crystallization. We thus could not follow time variation of the peak angles and intensities, from which the average size of the spherulites was usually estimated.

Nevertheless, the invariant Q defined in equation (1) for the *Hv* mode increases with time of cystallization, reflecting the increase in optical anisotropy as defined in equation (2). *Figure 2* shows the time variation of the reduced invariant Q_δ/Q_δ^∞ taken at 110°C for Sb-PET and that at three different temperatures from 110 to 130°C for Ge-PET. *Figure 3* compares Arrhenius plots, $1/\tau_{1/2}$ *versus* $1/T$, for the spherulite growth rate constants of these PETs taken in the range of temperature between 110 and 130°C.

We notice that the spherulite growth is very rapid in Sb-PET as compared to Ge-PET. The front factor for $1/\tau_{1/2}$ *versus* $1/T$ plots for Sb-PET is ten times larger than that for

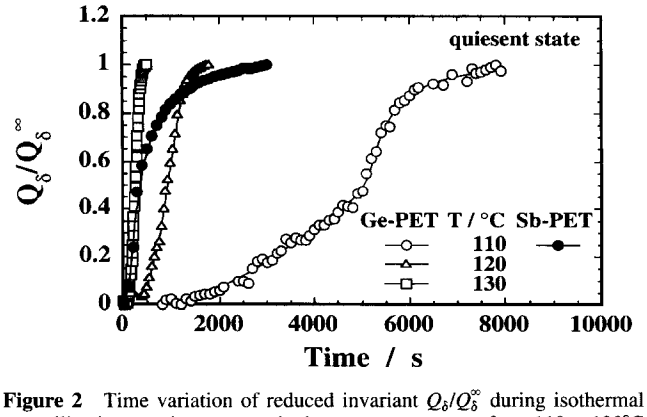

Figure 2 Time variation of reduced invariant Q_δ/Q_δ^∞ during isothermal crystallization at quiescent state in the temperature range from 110 to 130°C for Ge-PET and at 110°C for Sb-PET

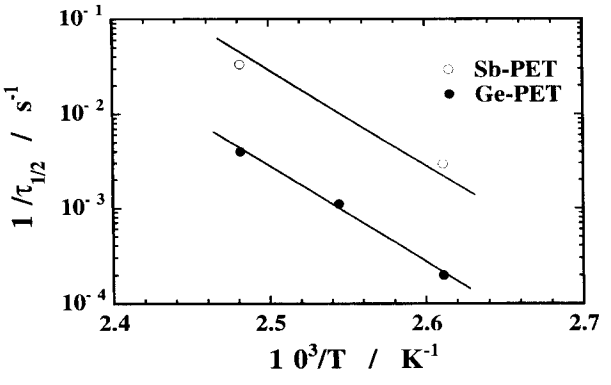

Figure 3 Temperature dependence of the reciprocal half-time of the spherulite growth $1/\tau_{1/2}$

Ge-PET, but the slope that reflects the activation energy of the crystallization process is virtually the same. The result implies that the number of nucleation sites is larger in Sb-PET, but in the following crystallization processes the mechanisms of the spherulite growth are virtually the same in both systems.

Elongational viscosity

We then attempted to determine, from transient tensile stress $\sigma(\dot{\varepsilon}_0;t)$ data, transient elongational viscosity $\eta_E(\dot{\varepsilon}_0;t)(\equiv \sigma(\dot{\varepsilon}_0;t)/\dot{\varepsilon}_0)$ as a function of Hencky strain rate $\dot{\varepsilon}_0$ and time t in the temperature range of 110–130°C covered in the isothermal crystallization experiments. However, above 120°C Sb-PET crystallized so fast that the specimen slipped between the metal belt clamps of EFOR and we could not determine $\eta_E(\dot{\varepsilon}_0;t)$ in this temperature range.

Thus for Sb-PET we collected data only at 110°C where the spherulite growth was reasonably slow and compared the results with those of Ge-PET taken at 100–130°C [1,2]. *Figure 4* compares the time variation of $\eta_E(\dot{\varepsilon}_0;t)$ for both Sb- and Ge-PET taken at 110°C with two different Hencky strain rates, $\dot{\varepsilon}_0 = 0.005$ and $0.01\ s^{-1}$. In both cases, $\eta_E(\dot{\varepsilon}_0;t)$ of Sb-PET is larger and exhibits a tendency of strain-induced hardening (or upward-deviation from the $\dot{\varepsilon}_0$-independent portion of the $\eta_E(\dot{\varepsilon}_0;t)$ curve) at an earlier up-rising time $t_{\eta E}$ than those of Ge-PET such as shown in *Figure 4* with the arrows.

In *Figure 5* we plotted $\dot{\varepsilon}_0$-dependence of $\varepsilon_{\eta E}(\equiv \dot{\varepsilon}_0 t_{\eta E})$ for Sb-PET at 110°C on the previously obtained $\varepsilon_{\eta E}(\equiv \dot{\varepsilon}_0 t_{\eta E})$ *versus* $\dot{\varepsilon}_0$ plots for Ge-PET taken at 100–130°C[1]. We see that Sb-PET at 110°C shows quite different behaviour as compared to Ge-PET at the same temperature, for which $\varepsilon_{\eta E}$ remains almost constant of around 1.0 in the whole range of $\dot{\varepsilon}_0$ examined. For Sb-PET elongated at 110°C $\varepsilon_{\eta E}$ decreases with decreasing $\dot{\varepsilon}_0$, which resembles the behaviour of

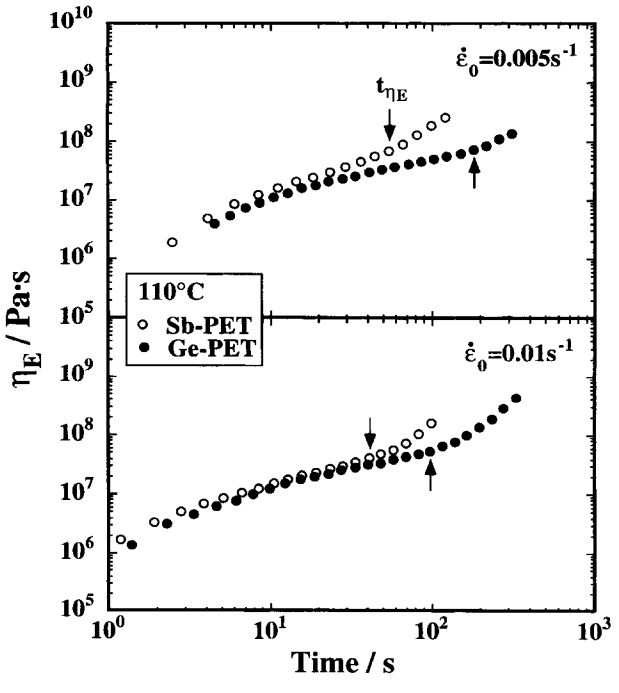

Figure 4 Comparison of elongational viscosity $\eta_E(t)$ *versus* time t curves between Sb- and Ge-PET elongated at 110°C with $\dot{\varepsilon}_0 = 0.005$ and 0.01 s^{-1}. The arrows indicate up-rising time $t_{\eta E}$ at which $\eta_E(t)$ begins to deviate from the linear, $\dot{\varepsilon}_0$-independent $\eta_E(t)$ *versus* t curves

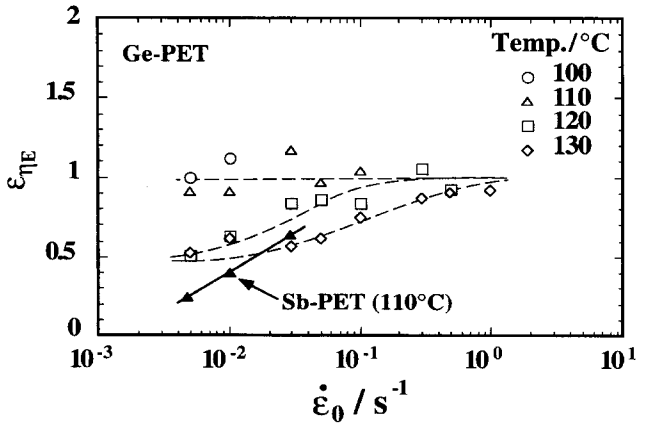

Figure 5 Strain rate $\dot{\varepsilon}_0$-dependence of up-rising Hencky strain $\varepsilon_{\eta E}$ ($=\dot{\varepsilon}_0 t_{\eta E}$) for PETs between 100 and 130°C

Ge-PET elongated at 130°C. These results suggest that in Sb-PET the gross crystallization rate is rapid even in the specimen under elongation with a large strain rate as will be demonstrated below.

Crystallization under elongation

Figure 6 shows TMd.s.c. data of Sb- and Ge-PET elongated at 110°C to various extents of Hencky strain. In *Figure 6* shown are: (a) Hencky strain ε *versus* cold crystallization temperature T_{cc} (that is the exothermic-peak or crystallization temperature during a heating process of d.s.c. which appears in the lower temperature side of the main crystallization peak in the nonreversing heat flow profile[1]); and (b) the endothermic heat flow ΔH_{diff} ($=\Delta H_{rev} - \Delta H_{nonrev}$) corresponding to the true degrees of crystallinity χ_c (bottom) calculated from TMd.s.c. run[1]. The true degrees of crystallinity χ_c, i.e. the crystallinity that has existed in the

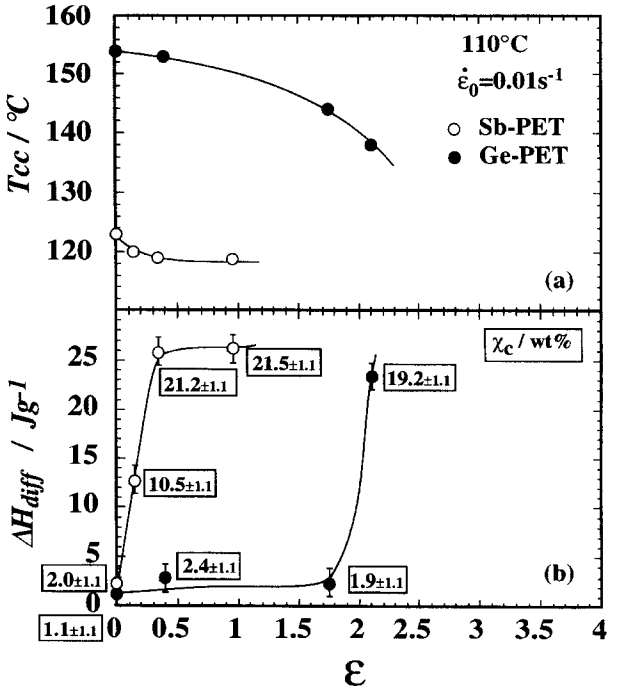

Figure 6 Plots of (a) cold crystallization temperature T_{cc} and (b) difference of the heat flow ΔH_{diff} for PETs for Sb- (open symbols) and Ge-PET (closed symbols) elongated at 110°C with $\dot{\varepsilon}_0 = 0.01$ s^{-1}. The degree of %-crystallinity χ_c of each specimen is shown with the number in the box

stretched specimen before the d.s.c. run was calculated as $\chi_c = \Delta H_{diff}/\Delta H^0$ with $\Delta H^0 = 122$ J g^{-1}, being the melting enthalpy of 100% crystalline PET[13]. In *Figure 6* the number in the box attached to each symbol represents the value of χ_c in wt%.

For Sb-PET, T_{cc} slightly decreases with increasing ε and remains constant around 120°C, whereas for Ge-PET, T_{cc} constantly decreases with ε as compared to that crystallized in the quiescent state. In Sb-PET spherulite growth surpasses and no change in χ_c is seen between a Hencky strain of 0.35 and 1.0, whereas in Ge-PET spherulite growth is neglible at 110°C so that nothing happens up until $\varepsilon = 1.75$, beyond which, however, flow-induced oriented crystallite formation takes place and χ_c reaches 19.2% at $\varepsilon \cong 2.1$, as reported in our previous paper (*cf.*, *Figure 6a*)[1,2]. The reduction in T_{cc} of Ge-PET implies that the quenched elongational-flow induced orientation of the segments make them easier to crystallize upon heating in the d.s.c. run.

These results suggest that quenched Ge-PET specimens once elongated to a high extent at low temperature are more easily crystallized during the d.s.c. heating process as compared to unstretched specimens. However, for Sb-PET the cold crystallization is nearly independent of the extent of elongation, implying that the spherulite structure has not been much affected during the elongation.

Birefringence and scattering patterns under elongation

Figure 7a shows birefringence $\Delta n(\varepsilon)$ *versus* ε curve for Sb-PET elongated at 110°C with $\dot{\varepsilon}_0 = 0.01$ s^{-1} and the relevant LS patterns. For comparison, we reproduce, in *Figure 7b*, similar data on Ge-PET elongated at 110°C from our previous paper[2]. For Sb-PET in an early stage of elongation up to $\varepsilon = 0.2$ with the degree of crystallinity of $\chi_c = 10.5$ wt% as revealed by TMd.s.c., a weak scattering pattern with slight anisotropy appears. Then the weak

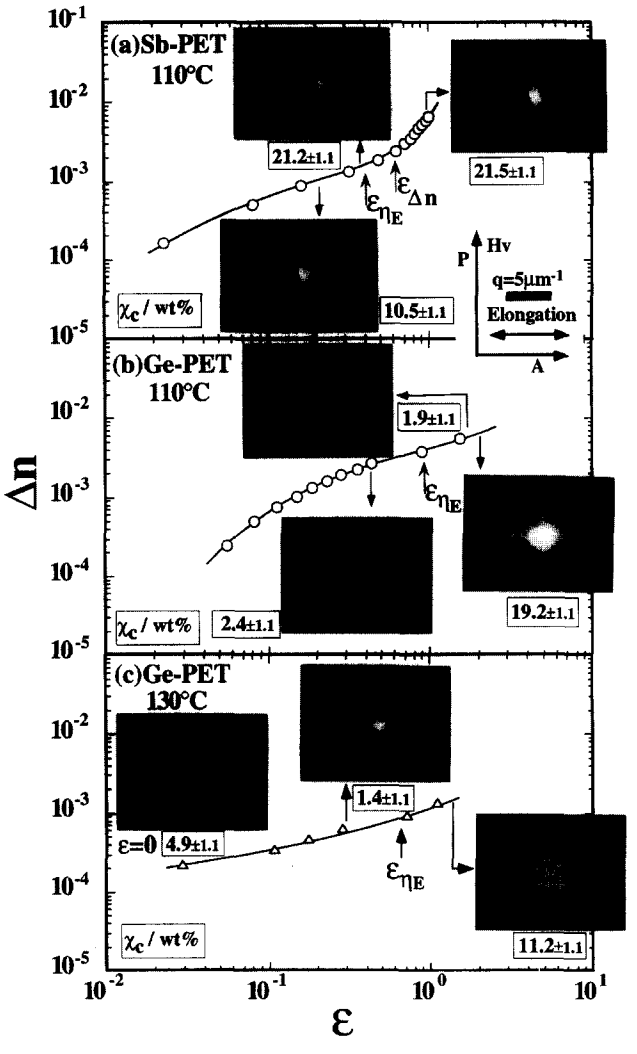

Figure 7 Double logarithmic plots of birefringence $\Delta n(t)$ *versus* Hencky strain ε ($=\dot{\varepsilon}_0 t$) and the relevant LS patterns for: (a) Sb-PET elongated at 110°C; (b) Ge-PET at 110°C; and (c) Ge-PET at 130°C with $\dot{\varepsilon}_0 = 0.01\ s^{-1}$. The degree of %-crystallinity χ_c of each specimen is shown with the number in the box

scattering pattern from Sb-PET specimen elongated to $\varepsilon = 0.35$ (where $\chi_c = 21.2$ wt%) just before strain-induced hardening prevails at $\varepsilon_{\eta E} = 0.42$ suggests the presence of rod-like crystalline aggregates[14]. The scattering pattern becomes more and more intense and clear, as the specimen is elongated through $\varepsilon = 0.6$ ($\cong \varepsilon_{\Delta n}$, the critical up-rising Hencky strain for birefringence at which Δn *versus* tensile stress curve deviates from the linear dependence) up to $\varepsilon = 1.0$ where χ_c remains constant at ~21 wt%. The LS pattern indicates development of rod-like morphology, suggesting that the transformation and rearrangement of new crystalline texture has taken place when the Sb-PET was elongated beyond $\varepsilon_{\Delta n}$ ($\cong 0.6$).

On the other hand, as seen in *Figure 7b* (and also *Figure 2* of our previous paper[2]), Ge-PET elongated at 110°C exhibits a weak scattering pattern without any anisotropy during elongation up to $\varepsilon \cong 1.7$, beyond which, however, the pattern exhibits strong streaks along the meridional direction perpendicular to the stretch direction. The result suggests that strong molecular orientation has proceeded along the stretch direction in the real space. Furthermore, at $\varepsilon \cong 2.1$, two strong spots appear in the direction parallel to the stretch direction, accompanying an abrupt increase in χ_c from to 19.2 wt% and slight increase in Δn. The strong two-spot pattern is an indication of elongational flow-induced oriented crystallite formation[2]. The same scattering pattern was observed under a depolarized optical alignment (Vv). These results imply that the crystalline texture essentially grows normal to the oriented chain. The crystallization behaviour of Sb-PET under elongation at 110°C is entirely different from that of Ge-PET elongated at 110°C, but resembles those elongated at, say, 130°C, where spherulite growth dominates also in Ge-PET.

In Ge-PET elongated at higher temperatures, spherulite growth may dominate so that the critical Hencky strain $\varepsilon_{\eta E}$ (<1) is dependent on $\dot{\varepsilon}_0$ and small especially in the specimen elongated with low $\dot{\varepsilon}_0$ as shown in *Figure 5* and discussed in our previous paper[1] (*cf.* figure 5 in Ref. 1). *Figure 7c* shows a $\Delta n(\varepsilon)$ *versus* ε curve for Ge-PET elongated at 130°C with $\dot{\varepsilon}_0 = 0.01\ s^{-1}$ and its light scattering patterns[2]. We observe a weak scattering with a slight anisotropy from the specimen before the start of elongation $\varepsilon = 0$ at 130°C. Because of the 90 s idle time before the start, spherulite formation starts in this specimen and reaches $\chi_c \cong 4.9$ wt%. As the specimen is elongated, spherulites continue to grow and a four-leaf-clover pattern eventually emerges at $\varepsilon \cong 0.3$ and becomes smeared but intensified as the specimen is further elongated to $\varepsilon \cong 1.3$ (the stretch ratio $\lambda \sim 3.7$). This is typical of the scattering patterns from growing spherulites[15]. At 130°C, spherulite growth takes place even in the liquid under elongation, although its morphology is slightly disturbed but a substantial deformation of the grown spherulites is unlikely as judged from the apparently constant azimuthal angle μ (~45°) of the spots with the maximum intensity. Therefore rapid increase in $\Delta n(\varepsilon)$ is not seen for Ge-PET as opposed to the case of Sb-PET elongated at 110°C with $\dot{\varepsilon}_0 = 0.01\ s^{-1}$ (*cf. Figure 7a*).

Stress optical coefficients

Now we turn our attention to the stress optical coefficients, especially of Sb-PET under elongation at 110°C, where spherulite growth is predominant. The stress optical rule states that a simple proportionality exists between the refractive index- and the anisotropic stress tensors of a molten polymer undergoing deformation[16,17]. Thus for polymer melt elongation the rule simply reads:

$$\Delta n(t) = C(t)\sigma(t) \qquad (3)$$

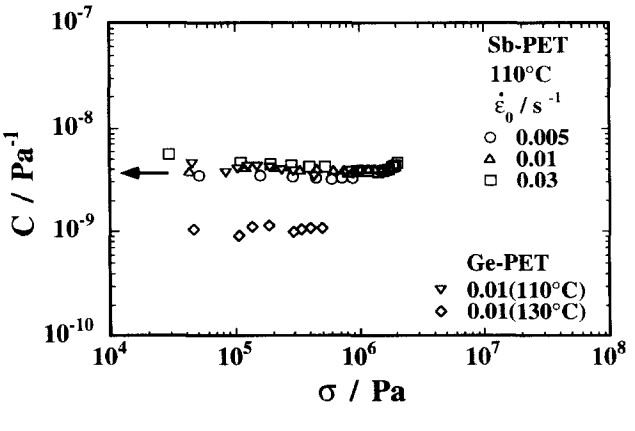

Figure 8 Double logarithmic plots of stress optical coefficient $C(t)$ *versus* tensile stress $\sigma(t)$ for Sb-PET elongated with three different strain rates $\dot{\varepsilon}_0 = 0.005$–$0.03\ s^{-1}$ at 110°C and for Ge-PET elongated with $\dot{\varepsilon}_0 = 0.01\ s^{-1}$ at 110 and 130°C. The arrow indicates the reported value of C ($=3.56 \times 10^{-9}\ Pa^{-1}$)

The stress optical coefficient $C(t) = \Delta n(t)/\sigma(t)$, first given by Treloar[18,19] for rubber elasticity, is supposed to be independent not only of time, ε or σ but also of $\dot{\varepsilon}_0$.

Figure 8 compares the $C(t)$ $(=\Delta n(t)/\sigma(t))$ *versus* $\sigma(t)$ curves of Sb-PET elongation taken at 110°C with three different $\dot{\varepsilon}_0$s from 0.005 to 0.03 s^{-1}, and those of Ge-PET elongation at 110°C and at 130°C with $\dot{\varepsilon}_0 = 0.01\ s^{-1}$. For Sb-PET elongation, the value of $C(t)$ agrees fairly well in the whole range of σ with the reported stress optical coefficient C $(=3.56 \times 10^{-9}\ Pa^{-1})$ for the rubbery component C_r of PET determined from dynamic shear flow experiments[20]. On the other hand, as seen in *Figure 8* for Ge-PET elongated at low temperatures, the $C(t)$ is again nearly constant up to $\sigma(t) \cong 10^6$ Pa, beyond which a slight upward deviation is seen. However, for those elongated at high temperatures, for example at 130°C, with a relatively low strain rate $\dot{\varepsilon}_0 < 0.01$, the value of C deviates downward below the reported value for shear deformation[1].

DISCUSSION

Strain-induced hardening versus crystallization behaviour

The results presented above clearly indicate that spherulite growth is a key factor governing the elongational flow rheology of supercooled PET liquids. Generally spherulite growth leads to an enhancement in σ and thus in $\eta_E(\dot{\varepsilon}_0;t)$ to an extent larger than that expected from the viscoelastic stress contribution. For a PET in which spherulite growth was dominant, we recognized that the critical Hencky strain $\varepsilon_{\eta E}$ ($\equiv \dot{\varepsilon}_0 t_{\eta E}$) for the onset of strain-induced hardening was strongly $\dot{\varepsilon}_0$-dependent. We thus examine the relation between $\varepsilon_{\eta E}$ and $\dot{\varepsilon}_0$ relative to the overall rate of crystallization that can be estimated *via* LS analysis under the quiescent state. Specifically we define the reciprocal, $1/\tau_{1/2}$, of crystallization half-time shown in *Figure 3* for the overall cystallization rate. *Figure 9* shows reduced plots of $\varepsilon_{\eta E}$ *versus* $\dot{\varepsilon}_0/(1/\tau_{1/2})$ constructed from $\varepsilon_{\eta E}$ *versus* $\dot{\varepsilon}_0$ data of *Figure 5* taken at different temperatures from 100 to 130°C.

We see that for Ge-PET all the data nicely conform to the reduced curve, in which $\varepsilon_{\eta E} \cong 1$ for $\dot{\varepsilon}_0 \cdot \tau_{1/2} > 100$, whereas the $\varepsilon_{\eta E}$ approaches 0.5 as $\dot{\varepsilon}_0 \cdot \tau_{1/2}$ is decreased well below 100. The estimated value of the critical dimensionless Hencky strain $(\dot{\varepsilon}_0 \cdot \tau_{1/2})_c$ is thus ~100. In the elongation of Ge-PET with a high strain rate of $\dot{\varepsilon}_0 \cdot \tau_{1/2} > 100$, elongational flow induced oriented crystallite formation overwhelms, and otherwise the spherulite growth dominates the strain-induced hardening behaviour.

On the other hand, for Sb-PET elongated at 110°C we could not attain a high enough $\dot{\varepsilon}_0 \cdot \tau_{1/2}$, so that elongational flow induced oriented crystallite formation might overwhelm. In the elongation at higher temperatures, the spherulite growth was too rapid to collect elongation data. Moreover, even in the elongation at low $\dot{\varepsilon}_0 \cdot \tau_{1/2}$ (< 10), the $\varepsilon_{\eta E}$ steadily decreases with decreasing $\dot{\varepsilon}_0 \cdot \tau_{1/2}$ and even appears to approach zero, as compared to the behaviour of Ge-PET. This result may be an indication that less stable spherulites in Sb-PET may be deformed in the early stage of elongation even at low $\dot{\varepsilon}_0 \cdot \tau_{1/2}$, although the spherulite growth rate is high. This feature may also be revealed through Rayleigh scattering studies on supercooled PET under elongation, as will be discussed in the next section.

Anyway the $(\dot{\varepsilon}_0 \cdot \tau_{1/2})_c$ is important in optimizing blow-moulding conditions of PET resins to obtain a transparent material containing a least amount of spherulites.

Through these approaches of evaluating $(\dot{\varepsilon}_0 \cdot \tau_{1/2})_c$ we may propose an optimum processing condition for blow moulding process of not only PET resins of different grades but also other semicrystalline polymer liquids in supercooled state.

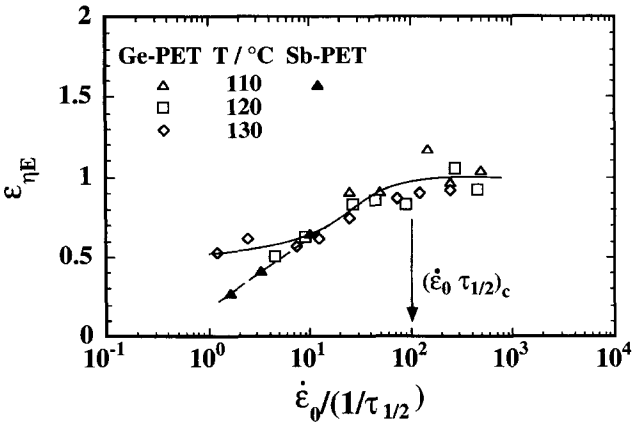

Figure 9 Reduced plots of $\varepsilon_{\eta E}$ vs. $(\dot{\varepsilon}_0 \cdot \tau_{1/2})$ for Sb-PET at 110°C and Ge-PET from 110 to 130°C. The arrow indicates critical (dimensionless) Hencky strain $(\dot{\varepsilon}_0 \cdot \tau_{1/2})_c (\cong 100)$

Crystalline morphology development under elongation

Figure 10a shows a typical scattering pattern for Sb-PET elongated at 110°C with $\dot{\varepsilon}_0 = 0.03\ s^{-1}$ up to $\varepsilon = 1.4$. In the figure we see two streaks with inclination α almost merge to one ($\alpha \cong 0$) and the robes decreasing their inclination β to 50°. These scattering patterns for Sb-PET including those shown in *Figure 7* can be modelled as in *Figure 10b*. These

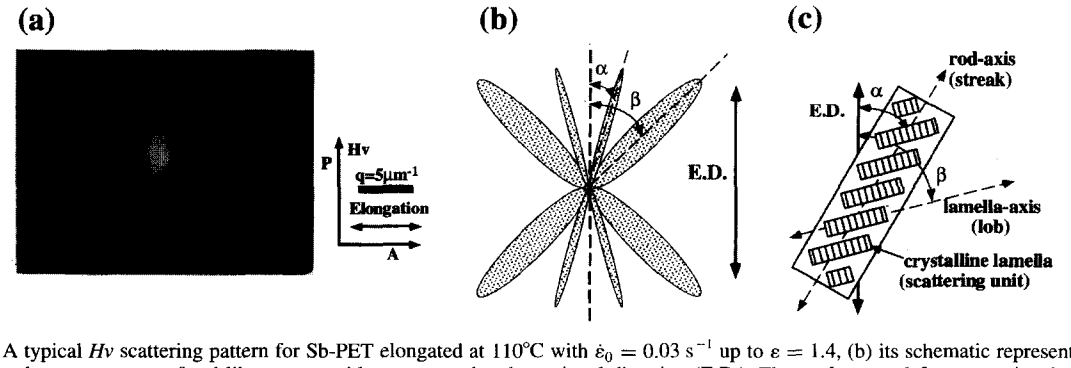

Figure 10 (a) A typical *Hv* scattering pattern for Sb-PET elongated at 110°C with $\dot{\varepsilon}_0 = 0.03\ s^{-1}$ up to $\varepsilon = 1.4$, (b) its schematic representation, and (c) a model describing the arrangement of rod-like texture with respect to the elongational direction (E.D.). The angles α and β are associated with the average orientation angle of the rods (the assembly of the lamellae) and that of the lamella axis, respectively, as depicted in the model

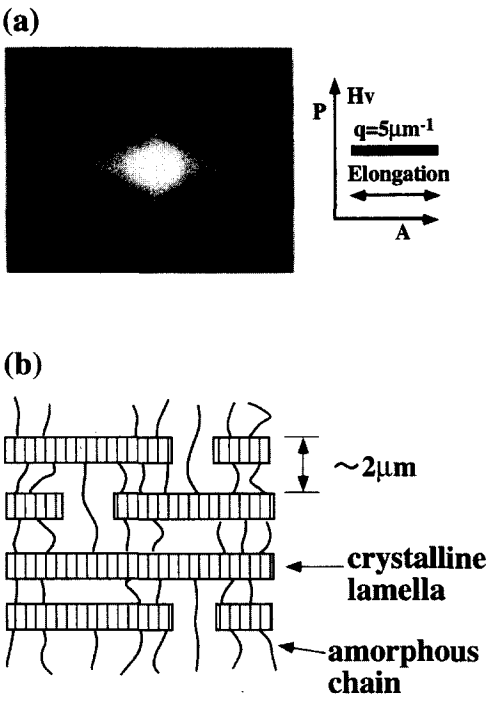

Figure 11 Typical example of (a) *Hv* light scattering pattern for elongational flow-induced oriented crystalline texture of Ge-PET elongated at 110°C with $\dot{\varepsilon}_0 = 0.01\ s^{-1}$ up to $\varepsilon \cong 2.1$ and (b) a crystalline texture model predicted from the *Hv* pattern

patterns consist of two parts: one is two split streaks inclined with an angle α and the other, two diffuse lobes inclined with an angle β to the direction of elongation in the real space. The model suggests that as depicted in *Figure 10c* a rod-like entity oriented with an angle α more or less parallel to the elongational direction as first proposed by Yau and Stein[21] some 30 years ago. The thin streaks may arise from the rods with inclination α which are supposed to be composed of stacked crystalline lamellae, while the thick lobes may arise from the scattering from the crystalline lamellae themselves with inclination β to the direction of elongation.

On the contrary, as seen in *Figure 7b* or *Figure 11a*, the scattering from Ge-PET elongated at 110°C up to $\varepsilon \cong 2.1$ yields a strong two-spot pattern, which is an indication of elongational flow-induced oriented crystallite formation. The same scattering pattern was observed under a depolarized optical alignment (Vv). These results imply that the crystalline texture essentially grows normal to the oriented chain as depicted in *Figure 11b*. That is, a lateral growth of the crystallites proceeds with elongation. We roughly estimated the scale as ~2 μm from the long period of the maximum peaks of the spots. In this case of Ge-PET elongated at 110°C, the slow spherulite growth rate leads to the flow-induced oriented crystalline formation, in which the chains are first oriented along the stretch direction and then the lamellae develop in the direction perpendicular to the stretch direction as depicted in *Figure 11b*.

In the elongation of Ge-PET at 130°C where the spherulite growth rate is high and the grown spherulite is rather stable, the four-leaf-clover pattern typical to the spherulites does not change its shape even at high ϵ, as seen in *Figure 7c*, implying that the spherulites are not very much deformed.

Stress optical rule for pet under elongation

Returning to the birefringence of Sb-PET under elongation, we notice that the $C(t)$ ($= \Delta n(t)/\sigma(t)$) *versus* $\sigma(t)$ curve for Sb-PET in *Figure 7a* shows a strong upward deviation at $\sigma(t) = 10^6$ Pa, corresponding to the critical Hencky strain $\varepsilon_{\Delta n} \cong 0.6$.

Comparing the $C(t)$ data with their scattering profiles shown in *Figure 10*, we speculate that the excess Δn or $C(t)$ may presumably arise from increasing orientation of crystalline lamellae during the elongation. As early as in 1956, Stein and Norris[22] interpreted the strain-induced birefringence of semicrystalline polymer solid by introducing contributions of crystalline and amorphous phases and the form birefringence due to the crystalline lamellae. Later for a crystalline rubber, Hashiyama *et al.*[23] proposed a new equation for estimating the contribution of the crystalline lamellae to the birefringence by neglecting the form birefringence but introducing the intrinsic birefringence Δn_c^0 and the orientation factor f_c of the crystalline lamellae, and applying the Guth–Smallwood expression[24] of the stress optical rule for rubber elasticity to the amorphous segments. Employing their method of analysis with the value of $\Delta n_c^0 = 0.22$ for PET proposed by Dumbleton[25], we estimated the change in the orientation factor f_c of the crystalline lamellae during elongation. The results, although not shown here, predicted a rapid increase in f_c beyond $\sigma = 10^6$ Pa, which semiquantitatively described the feature of the lamellae orientation found in Sb-PET (*cf. Figure 7a*).

In the elongation of Ge-PET at 110°C with $\dot{\varepsilon}_0 = 0.01\ s^{-1}$, $C(t)$ ($\cong 3.56 \times 10^{-9}\ Pa^{-1}$) is nearly constant for $\sigma(t)$ below 10^6 Pa, as seen in *Figure 9*. The result implies that under these conditions the flow induced-oriented crystalline formation did not take place and/or the enhancement in tensile stress and birefringence (due to the lamellae orientation) might have cancelled each other. On the other hand, in the elongation of Ge-PET at 130°C with $\dot{\varepsilon}_0 = 0.01\ s^{-1}$ where the spherulite growth was rapid, $C(t)$ began to deviate downward from the reported value for shear deformation. This result is indicative of the fact that the spherulite growth without accompanying strong orientation enhances the tensile stress but not very much the birefringence under these conditions.

CONCLUSIONS

We compared elongational flow-induced crystallization behaviour in rapidly crystallizable Sb-PET with that in slowly crystallizable Ge-PET in the temperature range commonly employed for the blow moulding operation. In Sb-PET during the elongation at 110°C, rapid growth of spherulites with low stability dominated in the early stage, and later transformation from the spherulites to a new crystalline texture, i.e. a rod-like structure occurred. The increase in Δn was due to the orientation of the crystalline lamellae toward the elongational direction.

In the case of slowly crystallizable Ge-PET elongated at 110°C, however, flow-induced orientation of the chain segments preceded until a critical Hencky strain of $\varepsilon \approx 2.0$, where oriented crystalline formation became prevailing, as revealed by TMd.s.c. and LS analyses. On the other hand, in the temperature range from 120 to 130°C, where spherulite growth in Ge-PET was substantial, the crystallization led to the strain-induced hardening and the reduction in C, reflecting strong enhancement in σ but rather weak enhancement in Δn due to the spherullite formation.

In the elongational flow of supercooled crystalline polymer liquids, obviously two mechanisms are competing, i.e. the flow-induced oriented crystalline formation and the spherulite growth. Which one of the mechanisms

overwhelms the rheology and birefringence is governed by whether the dimensionless reduced strain rate $\dot{\varepsilon}_0/(1/\tau_{1/2})$ is above or below a certain critical value ($\cong 100$ if $\tau_{1/2}$ is used), although the critical strain rate is dependent on a choice of a measure of the spherulite growth rate.

REFERENCES

1. Okamoto, M., Kubo, H. and Kotaka, T., *Polymer*, 1998, **39**, 3153.
2. Kubo, H., Sato, H., Okamoto, M. and Kotaka, T., *Polymer*, 1998, **39**, 501.
3. Kotaka, T., Kojima, A. and Okamoto, M., *Rheol. Acta*, 1997, **36**, 646.
4. Okamoto, M., Kojima, A. and Kotaka, T., *Polymer*, 1998, **39**, 2149.
5. Jabarin, S. A., *Polym. Eng. Sci.*, 1992, **32**, 1341.
6. Salem, D. R., *Polymer*, 1994, **35**, 771.
7. Lorentz, G. and Tassin, J. F., *Polymer*, 1994, **35**, 3200.
8. Tate, S., Watanabe, Y. and Chiba, A., *Polymer*, 1993, **34**, 4974.
9. Tate, S. and Ishimaru, F., *Polymer*, 1995, **36**, 353.
10. Okamoto, M. and Inoue, T., *Polymer*, 1995, **36**, 2739.
11. Okamoto, M., Shinoda, Y., Kinami, N. and Okuyama, T., *J. Appl. Polym. Sci.*, 1995, **57**, 1055.
12. Koberstein, J., Russel, T. P. and Stein, R. S., *J. Polym. Sci., Polym. Phys. Edn*, 1979, **17**, 1719.
13. Wunderlich, B., *Macromolecular Physics*, Vol. 3, Academic Press, New York, 1980.
14. Rhodes, M. B. and Stein, R. S., *J. Polym. Sci.*, 1969, **2A**(7), 1539.
15. Stein, R. S. and Rhodes, M. B., *J. Appl. Phys.*, 1960, **31**, 1873.
16. Janeschitz-Kriegel, H., *Polymer Melt Rheology and Flow Birefringence*, Springer Verlag, Berlin, 1983.
17. Doi, M. and Edwards, S. F., *The Theory of Polymer Dynamics*, Clarendon Press, Oxford, 1986, pp. 221–222.
18. Treloar, L. R. G., in *Die Physik Der Hochpolymeren*, ed. H. A. Stuart, Springer-Verlag, Berlin, 1956, Chap. 4.
19. Treloar, L. R. G., *The Physics of Rubber Elasticity*, 3rd edn, Clarendon Press, Oxford, 1975.
20. Inoue, M. and Osaki, K., *Abstract of the 8th Jpn Soc. Rheol. Symposium on Polymer Processing Technologies*, Nagoya, 1996, pp. 59–60.
21. Yau, W. and Stein, R. S., *J. Polym. Sci.*, 1968, **A2**(6), 1.
22. Stein, R. S. and Norris, F. H., *J. Polym. Sci.*, 1956, **21**, 381.
23. Hashiyama, M., Gaylord, R. and Stein, R. S., *Makromol. Chem., Suppl.*, 1975, **1**, 579.
24. Guth, E., *J. Appl. Phys.*, 1945, **16**, 20.
25. Dumbleton, J. H., *J. Polym. Sci.*, 1968, **A2**(6), 795.